Catalysis Today 143 (2009) 302–308

Contents lists available at ScienceDirect

Catalysis Today

journal homepage: www.elsevier.com/locate/cattod

Hybrid photocatalysts for the degradation of trichloroethylene in air

T.L.R. Hewer [b], S. Suárez [a,*], J.M. Coronado [a], R. Portela [a], P. Avila [c], B. Sanchez [a]

[a] CIEMAT-PSA Environmental Application of Solar Radiation Unit, Avda. Complutense 22, Building 42, 28040 Madrid, Spain
[b] Instituto de Química, Universidade de São Paulo-USP, C.P. 26077, CEP 05513-000, São Paulo, Brazil
[c] Institute for Catalysis and Petrochemistry, C/ Marie Curie 22, 28049 Madrid, Spain

ARTICLE INFO

Article history:
Available online 17 March 2009

Keywords:
Photocatalysis
TiO_2
Sepiolite
Hybrid photocatalyst
Trichloroethylene

ABSTRACT

Hybrid photocatalysts based on an adsorbent SiMgOx and a photocatalyst TiO_2 were developed in a plate shape. The ceramic surface was coated with TiO_2 by the slip-casting technique. The effect of the support in the photocatalytic degradation of trichloroethylene (TCE) was analyzed by modifying TiO_2 loading and the layer thickness. Photocatalysts were characterised by N_2 adsorption–desorption, mercury intrusion porosimetry, SEM, UV–vis spectroscopy and XRD. A direct relationship between the TiO_2 content and the photocatalytic activity was observed up to three layers of TiO_2 (0.66 wt.%). Our results indicate that intermediate species generated on the TiO_2 layer can migrate through relatively long distances to react with the OH^- surface groups of the support. By increasing the TiO_2 loading of the photocatalyst two effects were observed: trichloroethylene conversion is enhanced, while the efficiency of the oxidation process is decreased at expenses of increasing the selectivity to $COCl_2$ and dichloroacetylchloride (DCAC). The results are discussed in terms of the layer thickness, TiO_2 amount, TCE conversion and CO_2, and $COCl_2$ selectivity.

1. Introduction

Nowadays photocatalysis is a well-established technology for the abatement of pollutants, either in aqueous media or in the gas phase. TiO_2 is the most common material used in semiconductor photocatalyst because it is widely available at low prices and it possesses excellent photocatalytic properties. Generally, TiO_2 suspensions are preferred over supported catalysts because of the higher reaction rate of the former. For industrial applications, however, the development of supported photocatalysts is crucial. The immobilization of TiO_2 photocatalyst on a support avoids expensive filtration processes and the loss of the active component [1]. For this reason, the synthesis of immobilised photocatalytic materials is receiving a great deal of attention by both scientists and engineers [2,3]. Different materials such as glass, plastics and fibres are used as supports [4,5]. A more interesting approach consists in preparing hybrid photocatalysts, where adsorption and photocatalytic properties are combined, thus inducing a synergism towards the abatement of pollutants [6]. Physisorption of pollutants on the adsorbent part of the photocatalyst and their subsequent diffusion to the TiO_2 active sites results in an increase of the photocatalytic efficiency of this hybrid photocatalyst compared with traditional ones. Adsorbent with high surface area such as silica beads [7], pillared clays [8], mesoporous materials [9] and activated carbons [10,11] have been studied. The interaction between the adsorbent and the pollutant has to be controlled to allow pollutant diffusion to the interface between the adsorbent and the photoactive material.

Sepiolite is a natural magnesium silicate with a fibrous structure characterised by a high surface area, porosity and the capacity to include high quantity of water in the structure. This compound has been used in many applications [12–14]. Although it has been suggested that it can play a role in the diffusion of oxygen species and hydrogen spillover [15,16] the role of sepiolite is not fully understood.

On the other hand the diffusion through the air and solid phase of the OH radicals generated on illuminated TiO_2 has been reported for TiO_2 thin films on conventional supports [17]. Remote photodegradation of self-assembled monolayers of aliphatic chains anchored to an inert silicon surface and located at 20 μm away from the TiO_2 microdomains has been reported, demonstrating the diffusion ability of oxidizing species on the TiO_2 surface [18]. Remote oxidation of organic dyes separated from a TiO_2-coated plate by a small gap has also been proved [19].

The high quantum yield for trichloroethylene (TCE) degradation over TiO_2, which has been associated with the participation of chlorine [20] and hydroxyl radicals [21] as oxidative species in the reaction mechanism, has prompted the wide use of this compound as a model pollutant in photocatalytic studies [22–24]. The global oxidation pathway in the presence of water vapour is depicted in Eq. (1):

$$C_2HCl_3 + \frac{3}{2}O_2 + H_2O \rightarrow 2CO_2 + 3HCl \quad (1)$$

* Corresponding author. Tel.: +34 91 346 6177; fax: +34 91 346 6037.
E-mail address: silvia.suarez@ciemat.es (S. Suárez).

0920-5861/$ – see front matter © 2009 Elsevier B.V. All rights reserved.
doi:10.1016/j.cattod.2009.02.001

Nevertheless, the reaction is not as simple as represented in Eq. (1) and side reactions with the formation of different chlorinated products have been reported. Dichloroacetyl chloride (DCAC), phosgene ($COCl_2$) and molecular chlorine besides CO have been detected depending on operating conditions such as residence time and the water vapour partial pressure [25]. The complete mineralization cannot be accomplished in the absence of moisture and the formation of $COCl_2$, a very toxic compound, in addition to CO_2 is produced according to Eq. (2):

$$C_2HCl_3 + \frac{3}{2}O_2 \rightarrow COCl_2 + HCl + CO_2 \quad (2)$$

In a previous study, plate-shaped TiO_2–SiMgOx hybrid photocatalysts were prepared and tested for TCE degradation. TiO_2 was used in two different forms: in one case silicate and titania were mixed and extruded together; in a different approach, TiO_2 thick films were coated on previously extruded ceramic plates [26]. Materials obtained in both ways are referred to as incorporated and coated materials, respectively. The "corncob"-like structure of TiO_2–SiMgOx incorporated plates favoured the mineralization of TCE. Intermediate species photocatalytically generated in the TiO_2 nanoparticles may migrate through the adsorbent–photocatalyst interface to finally react with the numerous OH^- surface groups and adsorbed water molecules of the silicate. On coated samples, the migration through the TiO_2 thick films was supposed to be hindered.

Based on this working hypothesis, the aim of this work is to understand the role of the silicate as an active material in the photocatalytic process. Thus, sepiolite plates were coated with different number of TiO_2 layers from one to four modifying the TiO_2 amount and the layer thickness. The gap between the illuminated external surface where the photocatalytic process takes place and the interface where the reaction between intermediate species and OH^- groups occurs has been modulated.

2. Experimental

2.1. Catalyst preparation

Magnesium silicate (Tolsa S.A.) was used to prepare the ceramic plates. The composition of the magnesium silicate, expressed as oxides, was SiO_2: 59.50%, MgO: 17.55%, Al_2O_3: 6.26%, CaO: 2.36 wt.%, Fe_2O_3: 1.84 wt.%, Na_2O: 0.53 wt.%, K_2O: 1.73 wt.%. The powder samples were mixed and kneaded with water until a ceramic dough with the optimal plasticity was obtained [27]. The plates were obtained by extrusion using a specifically designed die. Fresh samples were dried at room temperature for 7 days, then at 110 °C for 24 h and finally heat-treated at 800 °C for 4 h. The resulting plates presented the following dimension: 8.0 cm × 2.9 cm × 0.25 cm (length × width × thickness).

Commercial TiO_2 (G-5 Millenium) with purity higher than 98% and a sulphate content between 0.8 wt.% and 1.7 wt.%, P_2O_5 <0.4 wt.% and Na_2O and K_2O <0.01 wt.% were selected to prepare the aqueous suspension. A water dispersion of TiO_2 (30 g L^{-1}) acidified with 1 M HNO_3 was prepared by prolonged sonication to improve the dispersion in the aqueous media. The SiMgOx plates treated at different temperatures were immersed in the TiO_2 suspension by the slip-casting technique at a constant rate of 3 mm s^{-1}. Four samples were prepared by varying the number of coatings from one to four, drying the samples after each coating at 100 °C for 1 h. The materials were finally heat-treated at 500 °C for 4 h. The surface of the support covered by TiO_2 was around 20.0 cm^2. The photocatalysts were named as SiTi-*x* where *x* indicates the number of TiO_2 layers.

2.2. Physicochemical characterisation

The specific surface area (S_{BET}) of the samples was calculated from nitrogen adsorption at −196 °C determined with a Carlo Erba Sorptomatic 1800, outgassing the samples overnight using oil-diffuser and rotatory pumps at 300 °C to a pressure of $<1.33 \times 10^{-2}$ Pa to ensure a dry clean surface, free from any loosely bound adsorbed species. The pore volumes were analyzed by use of *Mercury Intrusion Porosimetry* (MIP) using CE Instruments Pascal 140/240 porosimeter, after drying the samples at 150 °C overnight. The total pore volumes were determined by combinations of nitrogen adsorption and mercury intrusion analysis.

X-ray diffraction (XRD) patterns of ground samples of the monolithic catalyst were recorded on a Phillips PW1710 powder diffractometer using Cu Kα radiation: λ = 0.154 nm, sampling data every 0.02° (2θ) at an acquisition rate of 2 s/step. The mean TiO_2 particle size was determined from Scherrer's equation with the normal assumption of spherical crystallites. The anatase phase content was determined from peak intensity of the most intense diffraction peak (1 0 1) at 25.4°. UV–vis absorption spectra of the plates were collected with a LAMBDA 950 UV-Vis-NIR spectrophotometer between 2500 nm and 300 nm wavelength with 10 nm step.

Scanning electron microscopy and energy dispersive X-ray spectroscopy studies were performed in a Zeiss DSM 960 Digital Scanning Microscope with a Si/Li detector and a Be window of 7 μm thickness, coupled with an analyzer of dispersive energies EXD Link eXL with a 25 keV electron beam and a take-off angle of 45°. Samples were coated with a conductive layer of graphite to minimize charging effects.

2.3. Photocatalytic tests

The photocatalytic oxidation of trichloroethylene (TCE) was studied in a continuous plug flow gas-phase flat photoreactor. The photoreactor with external dimensions 120 mm × 50 mm × 10 mm (length × wide × thickness) was made of stainless steel except for one face where a window of 27 cm^2, made of pyrex glass, was placed for the photocatalyst illumination provided by two UVA Philips TL-8W/05 fluorescent lamps with a maximum emission at 365 nm wavelength and light intensity 4.4 mW cm^{-2} with a Cole Parmer Radiometer VLX3W. A gas mixture of TCE and air was prepared using gas cylinder of TCE/N_2 (Air Liquide, 500 ppm) and compressed air free of water and CO_2. The flow rate was controlled by using electronic mass flow controllers. The TCE concentration was kept at 90 ppm, and the total gas flow between 240 mL min^{-1} and 700 mL min^{-1}. The gas composition was monitored continuously using a FTIR Thermo-Nicolet 5700 spectrometer, provided with a temperature controller multiple reflection gas cell (optical path 2 m) maintained at 110 °C. Gas cylinders of CO_2 (100 ppm Air Liquid) and $COCl_2$ (50 ppm Air Liquid) were used as references to determine the concentration of these compounds during the photocatalytic tests.

3. Results and discussion

The main characteristics of the hybrid photocatalysts based on sepiolite and covered with different amounts of TiO_2 are collected in Table 1. The TiO_2 concentration was set between 0.32 wt.% and 0.75 wt.%. A photograph of the silicate plate used as support and after deposition of four layers of TiO_2 is shown in Fig. 1. The method used for TiO_2 deposition ensures the formation of a homogeneous semitransparent film totally covering the surface. TiO_2 G-5 treated at 500 °C presented a BET area of 152 m^2 g^{-1} and an average crystal size of 16 nm. The sepiolite selected for this study and treated at 800 °C has a meso-macro structure with a total pore volume of 0.52 cm^3 g^{-1} and a mean pore diameter centred at 40 nm [26]. This

Table 1
Characteristics of the coated photocatalysts.

	No. of coatings	[TiO_2] (wt.%)	TiO_2/area[a] (mg cm^{-2})	Layer thickness (μm)	Reflectance (%) 400 nm
SiMgOx	–	–	0	–	29.6
Si/Ti-1	1	0.32	1.15	1	38.87
Si/Ti-2	2	0.55	1.95	3.8	43.2
Si/Ti-3	3	0.66	2.43	6.6	45.9
Si/Ti-4	4	0.75	2.64	10	50.0
TiO_2 G-5 fresh powder	–	100	–	–	89.6

[a] Considering the surface covered by TiO_2 (between 20.0 cm^2 and 21.0 cm^2).

structure, where macropores are generated by packing of the sepiolite fibres allows the fixation of TiO_2 in its surface. The BET area of the material treated at 500 °C is larger than that of the sample treated at 800 °C, 126 $m^2\ g^{-1}$ vs. 68 $m^2\ g^{-1}$. Nevertheless, the photocatalytic activity of the latter sample is higher than that of the one treated at 500 °C, at the same TiO_2 loading [26]. The high porosity of the support treated at low temperature results in the incorporation of TiO_2 inside the porous structure; those sites are not accessible to the UV radiation photons, lowering thus the photocatalyst efficiency. Thus, the selected temperature for the support treatment was 800 °C. Due to the low TiO_2 amount, modifications of textural properties were not observed with increasing the number of layers. The adsorption capacity measured in dynamic conditions was 2.2 μmol_{TCE}/g SiMgOx, using a total flow of 300 mL min^{-1} and 150 ppm TCE concentration.

Fig. 2 depicts the variation of the TiO_2 loading after consecutive layer deposition and the calculated arithmetic mean value for the SiTi-*x* composites. A progressive decrease of the TiO_2 loading with each deposition was observed. During the first coating around 0.27 wt.% of TiO_2 was taken, but only 0.15 wt.% was fixed in the third step. These results suggest that the porous structure of the adsorbent was progressively filled with titania particles. When the number of layers was above 4, the formation of flakes on the surface with poor adherence to the substrate was observed.

The TiO_2 G-5 sample treated at 350 °C, 500 °C and 800 °C was characterised by XRD. The diffractograms are shown in Fig. 3. TiO_2-anatase was the only crystalline phase detected. As expected, an increase of the crystal size from 11 nm to 47 nm was attained when the temperature increased from 350 °C to 800 °C. The temperature selected for the final treatment of the coated materials was 500 °C since it yields a relatively large surface area and a particle size of 16 nm improving the immobilization of TiO_2 onto the support.

In order to analyze the thickness of the TiO_2 layer, SEM analyses were performed for all the samples. Because of the ceramic nature of the support the TiO_2 layer can be easily detached from the surface during the polished process. Then, a sandwich-like structure with a resin between two pieces of the sample was used to fix the TiO_2 coating on the surface. Once the resin was dried, the face selected for the analysis was polished. A SEM micrograph of the plate's cross-section along to the TiO_2 line profile for the sample prepared with four TiO_2 layers is shown in Fig. 4a. From the left part of the micrograph to the right the different components of the composite can be distinguished: silicate, TiO_2 layer, resin (black zone in the middle), TiO_2 layer and silicate. The line profile showed around 35 μm and 70 μm

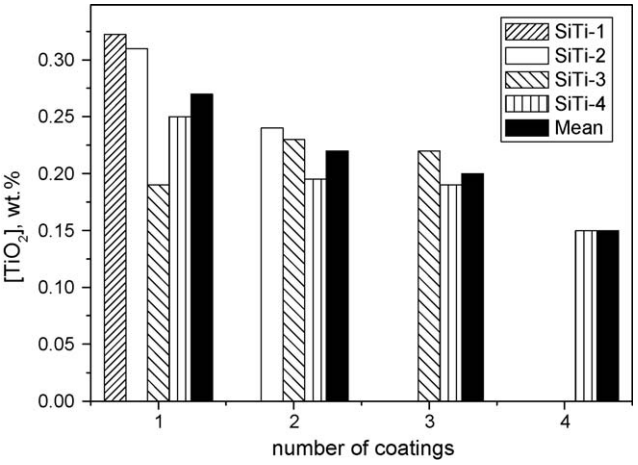

Fig. 2. Variation of the amount of TiO_2 deposited on the substrate with the number of layers.

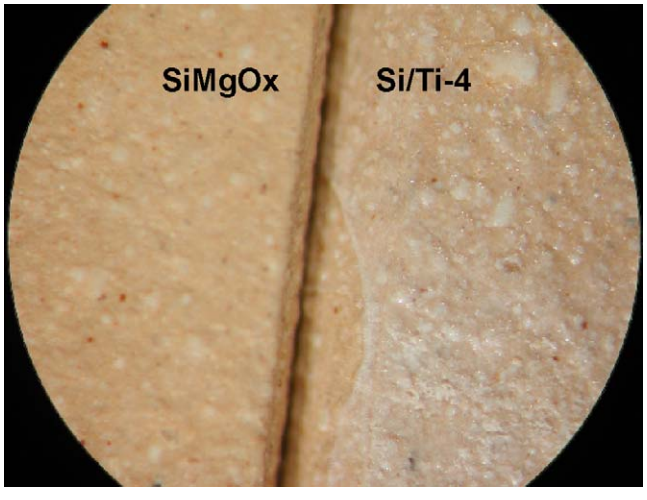

Fig. 1. Photograph of magnesium silicate plate treated at 800 °C and Si/Ti-4 hybrid photocatalysts with four layers of TiO_2.

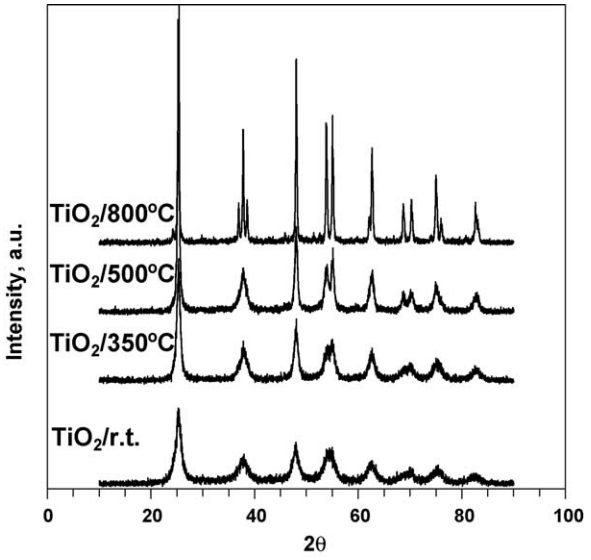

Fig. 3. XRD diffractograms of TiO_2 G-5 treated at different temperatures.

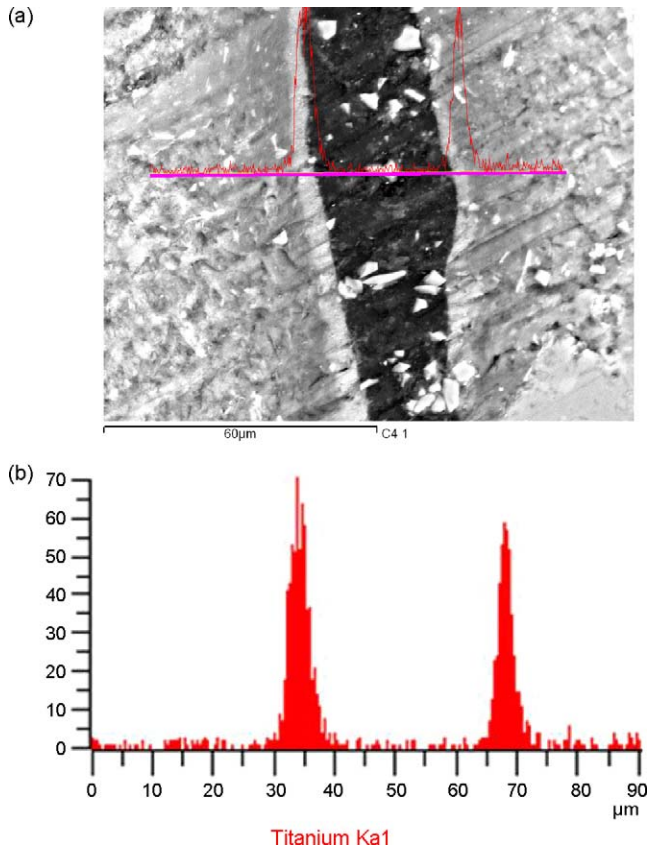

Fig. 4. (a) Micrography of a sandwich-like structure cross-section obtained by SEM, and (b) Ti analysis obtained by XEDS from Si/Ti-4.

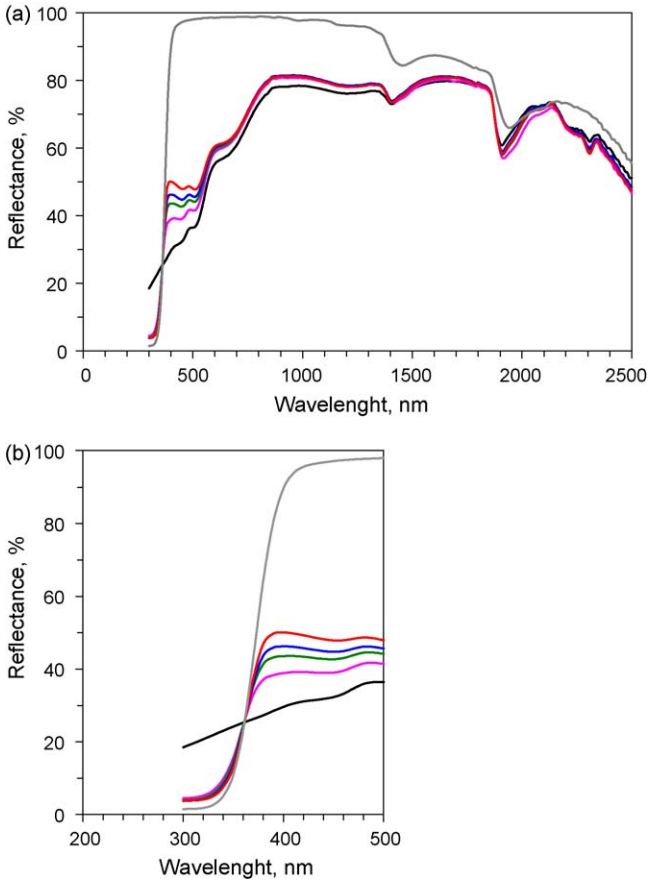

Fig. 5. (a) UV–vis spectra in the region between 300 nm and 2500 nm and (b) magnification of the region between 300 nm and 500 nm for the raw materials and coated samples: TiO_2 G-5 r.t. (grey), SiMgOx (blank), Si/Ti-1 (pink), Si/Ti-2 (green), Si/Ti-3 (blue), and Si/Ti-4 (red). (For interpretation of the references to color in this figure legend, the reader is referred to the web version of the article.)

titanium-rich areas with a mean layer thickness around 10 μm (see Fig. 4b). Analyses of 20 different regions give us an estimation of the mean layer thickness of the each sample. From the results shown in Table 1 it can be observed that the thickness of the layers varies from 1 μm to 10 μm. After deposition of four TiO_2 layers, the fibrous structure of the silicate cannot be distinguished at composite external's surface. Only sphere-shaped particles due to TiO_2 aggregates covering the surface are observed, 80% of the particles displaying sizes between 120 nm and 320 nm [26,28].

The reflectance spectra obtained by UV–vis-NIR spectroscopy for sepiolite, TiO_2, and SiTi-*x* photocatalysts are depicted in Fig. 5. Bands centered at 1400 nm, 1910 nm and 2300 nm were detected in the sepiolite. Framework silicates such as quartz have no prominent absorption features in the UV–vis-NIR [29]. The bands at 1400 nm and 1900 nm can be ascribed to contributions from vibrational combination and overtones of molecular water contained in the material. The spectrum is characteristic of a water-rich material showing an intense absorption band at 1900 nm due to the combination of the H–O–H bending and O–H stretching modes [30,31]. The structure of the sepiolite with channels between the Si and Mg sheet in tetrahedral and octahedral coordination allows the incorporation of a significant amount of water in the channels. Less pronounced absorption peaks also appear at 1400 nm and 2300 nm. The band at 1400 nm is the typical first overtone of the O–H stretch. Moreover the band at 2300 nm is the combination of Mg–OH bending, O–H stretching combination and Al–OH bend in minor proportion. Two bands can be observed in the visible region, at 430 nm and 500 nm, probably due to the presence of iron in the sample [32]. Bands at 2100 nm and 2200 nm may be assigned to carbonates present in the magnesium silicate.

In Fig. 5b a magnification of the region between 300 nm and 500 nm is represented. At 300 nm the reflectance of TiO_2 containing samples was closed to zero because of TiO_2 band-gap absorption. At this point sepiolite reflects around 20% of the radiation. Differences on the reflectance of SiTi-*x* composites with the number of coatings were detected at wavelength above this value. The reflectances obtained at 400 nm wavelength with the number of coatings are summarised in Table 1. The surface of sepiolite was progressively covered with TiO_2 particles increasing the reflectance lineally with the TiO_2 amount from 28.9% to 50.0% for Si/Ti-1 and Si/Ti-4 respectively. The extrusion of a flat plate made entirely with TiO_2 was not possible, and the presence of a binder such as sepiolite is required. Nevertheless, the spectra of TiO_2 G-5 fresh powders sample were recorded as a reference point using a powdered sample holder. A reflectance of 90% at 400 nm was obtained. The strong increase compared to Si/Ti-4 was associated to the differences in the physicochemical characteristic of the materials used.

3.1. Photocatalytic activity results

In order to detect variations in the selectivity of the reaction products, photocatalytic tests were carried out in the absence of water vapour. The influence of the TiO_2 loading, which varies with the number of coatings, in the TCE conversion with the total gas flow was investigated. In Fig. 6 the TCE conversion as well as the amount of the reaction products detected in the outlet is shown. By lowering the contact time, a decrease of the photocatalytic activity, is observed in accordance with previous results [26]. The results showed that at 300 mL min^{-1} all samples except Si/Ti-1 reached a

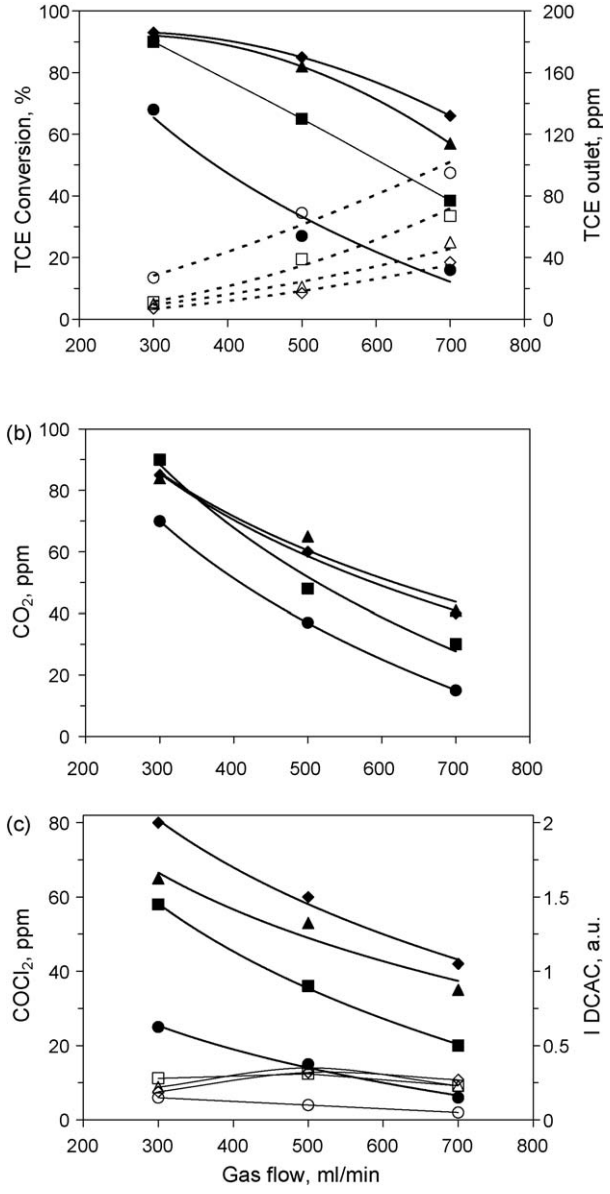

Fig. 6. Photocatalytic degradation of TCE and concentration of reaction products: (a) (filled symbols) TCE conversion and (open symbols) TCE amount, (b) CO_2, and (c) $COCl_2$ (filled symbols) and DCAC (open symbols) for (●) Si/Ti-1, (■) Si/Ti-2, (▲) Si/Ti-3, and (◆) Si/Ti-4.

90% of TCE conversion. As expected, higher TiO_2 amount yields faster reaction rates at high gas flow. For Si/Ti-1, Si/Ti-2 and Si/Ti-3 reaction rate constant values of 0.58×10^{-3} μmol s^{-1} cm^{-2}, 1.13×10^{-3} μmol s^{-1} cm^{-2} and 1.49×10^{-3} μmol s^{-1} cm^{-2} were reached at 500 mL min^{-1} respectively (referred to the geometric area of the support of 22.5 cm^2). Nevertheless a progressive increase of the rate with the total flow was observed for SiTi-4, which achieves values of 1.64×10^{-3} μmol s^{-1} cm^{-2} at 700 mL min^{-1}.

A strong influence of the TiO_2 amount in the activity at low TiO_2 concentration was observed. Thus, an increase of the TiO_2 content from 0.32 wt.% to 0.55 wt.% resulted in an increase of the TCE conversion around 40%. On the other hand only a slight influence of the TiO_2 content on the photocatalytic activity was observed for SiTi-3 and SiTi-4. As a matter of fact, these samples display similar performance being the most active of the series. The deposition of four layers of TiO_2 is near the highest loading that still permits an effective use of the UV radiation. Above 10 μm the formation of flakes on the TiO_2 layer took place. Then, the TiO_2 layer was flaking, avoiding the deposition of higher TiO_2 amount.

For comparative purposes a sample prepared with TiO_2 sol–gel with four layers on a borosilicate plate [33] was tested under similar conditions. A 35% of TCE conversion was attained at 300 mL min^{-1} and only 8% at 700 mL min^{-1}. In spite of structural differences between these systems such as particle size, BET area or TiO_2 loading, the superior catalytic performance of the hybrid composites reveals the advantage of the combination of adsorption and photocatalytic properties in a single material, by allowing the treatment of a large gas volume at relative high concentration of pollutant.

A decrease of the CO_2 and $COCl_2$ amount with contact time was also observed (Fig. 6b and c) with a slight increase in the formation of DCAC, except for Si/Ti-1 where the DCAC was close to zero. According to Blake and co-workers [25], the formation of DCAC and $COCl_2$ can be considered as consecutive reactions. Thus, longer residence times favour the reaction of DCAC to $COCl_2$ explaining the higher $COCl_2$ quantities [26]. An important dependence of the $COCl_2$ concentration with TiO_2 loading was observed.

The calculation of the CO_2 and $COCl_2$ selectivity should be included in all the reaction products observed in the reaction. Taking into account that in our case the main reaction products detected were CO_2 and $COCl_2$, the selectivity to CO_2 and $COCl_2$ was estimated according to the carbon balance shown in Eqs. (1) and (2). Thus, the CO_2 selectivity was calculated according to the following equation:

$$S_{CO_2} = \frac{CO_2}{(TCE_{inlet} - TCE_{outlet})2} \times 100 \quad (3)$$

These data are shown in Fig. 7. The CO_2 selectivity decreases in the following order: SiTi-1 ≫ SiTi-2 > SiTi-3 > SiTi-4 and the $COCl_2$ selectivity follows the opposite trend. Although SiTi-4 sample was the most active material in terms of conversion, it was also the one that displayed the highest selectivity to $COCl_2$ at the lowest residence time.

The selectivity to CO_2, $COCl_2$ at 90% TCE conversion (total flow of 300 mL min^{-1}) was analyzed. As the amount of TiO_2 increases with the number of layers, the selectivity to CO_2 decreases; on the contrary a higher selectivity to $COCl_2$ was observed. These results outline the key role that the interface between the two materials plays in the TCE mineralization. A short distance between the external surface of the TiO_2 layer where the photocatalytic reaction occurs and the substrate favours CO_2 formation.

Blake and co-workers [34] proposed that the reaction proceeds through a DCAC intermediate Eq. (4). Then, DCAC reacts to produce the different reaction products. One possible reaction is the formation of $COCl_2$ as shown in Eq. (5). A direct oxidation pathway has also been proposed based on the fact that the oxidation of DCAC in air produces a different proportion of products than that observed during the oxidation of TCE [25]. As it was explained before, TCE mineralization reaction in the absence of water vapour produces a large quantity of $COCl_2$. But according to Eq. (6), $COCl_2$ can undergo hydrolysis reaction in the absence of light to produce CO_2. Complete and quantitative hydrolysis of $COCl_2$ to CO_2 with activated carbon pellets has been achieved by these authors.

$$C_2HCl_3 + \frac{1}{2}O_2 \rightarrow C_2HCl_3O \quad (4)$$

$$C_2HCl_3 + \frac{1}{2}O_2 \rightarrow COCl_2 + HCl + CO \quad (5)$$

$$COCl_2 + H_2O \rightarrow CO_2 + 2HCl \quad (6)$$

When the contact time was below 0.6 s (obtained at 500 mL min^{-1}), TCE could hardly adsorbed on the actives sites and a decrease in the concentration of all reaction products was

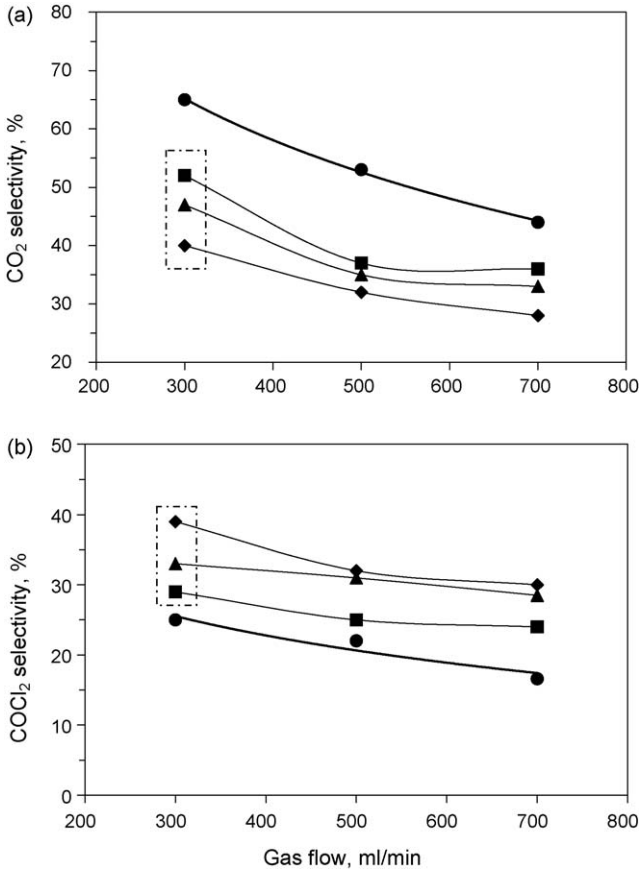

Fig. 7. (a) CO_2 and (b) $COCl_2$ selectivity in the TCE photodegradation reaction for (●) Si/Ti-1, (■) Si/Ti-2, (▲) Si/Ti-3, and (◆) Si/Ti-4.

observed. Above this value, adsorbed DCAC has enough time to react with oxygen to produce $COCl_2$ and CO_2. The results shown in Fig. 7 indicate that high TiO_2 loading due to larger thickness produced an increase in the $COCl_2$ formation probably because the reaction with the OH surface groups of the adsorbent was not favoured. Nevertheless, for low TiO_2 layer thickness, the migration of the reaction intermediates and the subsequent reaction with the OH groups of the silicate was promoted. These data support previous result where it was proposed that incorporated hybrid photocatalysts showed the highest CO_2 selectivity compared to sample prepared by coating [26]. The results obtained in the current study sustain the idea that an intimate contact between sepiolite fibres and TiO_2 with a corncob-like structure improves TCE mineralization.

The scheme represented in Fig. 8 illustrates the process-taking place in the surface of the photocatalysts. At low TiO_2 loading or thin TiO_2 layer (left) the intermediate species can easily migrate through the layer to the interface between the TiO_2 and the substrate. Thus the reaction between intermediate products such as $COCl_2$ and OH surface groups or adsorbed water molecules of the silicate can take place increasing TCE mineralization. On the other hand, when the TiO_2 layer thickness increase (right), even if the TCE degradation rate is faster, the migration of these intermediate species is hindered by the long gap between the adsorbent and the catalytic surface where the reaction occurs. Consequently a decrease in TCE mineralization is observed.

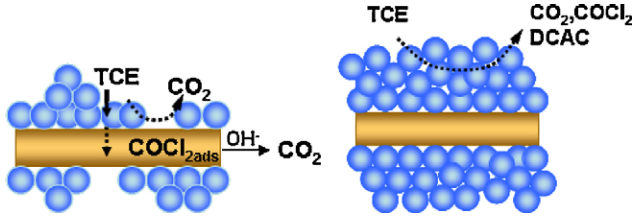

Fig. 8. Schematic proposed for degradation of TCE on coated hybrid photocatalysts with different TiO_2 layer thicknesses: (○) TiO_2 photoactive particles and (□) sepiolite support.

4. Conclusions

The results of this work evidence the key role of the support on the photocatalytic mineralization of TCE. This improvement accounts to its adsorption capability and the presence of OH^- surface groups which are essential to carry out the trichloroethylene photocatalytic oxidation reaction. In spite of the direct relationship between TiO_2 loadings and reaction rate, the TiO_2 layer thickness has an important influence on the catalysts selectivity. When the distance between the external surface where the photocatalytic reaction tales place and the adsorbent increase, the diffusion of intermediates species is hindered, resulting in a pronounced decrease of the selectivity to CO_2. It is in this interface where intermediate species react with OH groups of the support favouring TCE mineralization. In order to optimise the performance of coated hybrid photocatalysts several parameters have to be considered. Besides the factor related to the TiO_2 physicochemical properties, the thickness of the layer plays an important effect on the selectivity of the process when hybrid photocatalysts are used.

References

[1] O. Carp, C.L. Huisman, A. Reller, Prog. Solid State Chem. 32 (2004) 33.
[2] J.C. Yu, L. Zhang, Z. Zheng, J. Zhao, Chem. Mater. 15 (2003) 2280.
[3] Y. Chen, D.D. Dionysiou, Appl. Catal. B 80 (2008) 147.
[4] R. Portela, B. Sánchez, J.M. Coronado, R. Candal, S. Suárez, Catal. Today 129 (2007) 223.
[5] B. Herbig, P. Löbmann, J. Photochem. Photobiol. A: Chem. 163 (2004) 359.
[6] N. Takeda, T. Torimoto, S. Sampath, S. Kuwabata, H. Yoneyama, J. Phys. Chem. 99 (24) (1995) 9986.
[7] L. Zou, Y. Luo, M. Hooper, E. Hu, Chem. Eng. Process. 45 (2006) 959.
[8] C. Ooka, H. Yoshida, K. Suzuki, T. Hattori, Appl. Catal. A 260 (1) (2004) 47.
[9] D.G. Shchukin, D.V. Sviridov, J. Photochem. Photobiol. C: Photochem. Rev. 7 (2006) 23.
[10] Y. Gao, H. Liu, Mater. Chem. Phys. 92 (2005) 604.
[11] H. Yoneyama, T. Torimoto, Catal. Today 58 (2000) 133.
[12] J. Blanco, A.L. Petre, M. Yates, M.P. Martin, S. Suárez, J.A. Martin, Adv. Mater. 18 (9) (2006) 1162.
[13] A. Arques, A.M. Amat, L. Santos-Juanes, R.F. Vercher, M. Martín, A.J. Miranda, Mol. Catal. A 271 (1–2) (2007) 221.
[14] R. Fernández-Saavedra, P. Aranda, E. Ruiz-Hitzky, Adv. Funct. Mater. 14 (1) (2004) 77.
[15] S. Suárez, M. Yates, A.L. Petre, J.A. Martín, P. Avila, J. Blanco, Appl. Catal. B 64 (3–4) (2006) 302.
[16] P. Baeza, M. Villarroel, P. Avila, A.L. Agudo, B. Delmon, F.J. Gil-Llambias, Appl. Catal. A 304 (2006) 109.
[17] M.C. Lee, W. Choi, J. Phys. Chem. B 106 (45) (2002) 11818.
[18] H. Haick, Y. Paz, J. Phys. Chem. B 105 (15) (2001) 3045.
[19] T. Tatsuma, S. Tachibana, T. Miwa, D.A. Tryck, A. Fujishima, J. Phys. Chem. B 103 (38) (1999) 8033.
[20] M.R. Nimlos, W. Jacoby, D.M. Blake, T.A. Milne, Environ. Sci. Technol. 27 (4) (1993) 732.
[21] S.H. Teichner, M. Formeti, in: M. Schiavello, D. Reidel, (Eds.), Photoelectrochemistry, Photocatalysis and Photoreactors, Dordrecht, Holland 1985, pp. 457–489.
[22] J.F. Kenneke, J.L. Ferry, W.H. Glaze, in: D.F. Ollis, H. Al-Ekabi (Eds.), Photocatalytic Purification and Treatment of Water and Air, Elsevier Science Publishers, Amsterdam, 1993, p. 179.
[23] L.A. Dibble, G.B. Raupp, Catal. Lett. 4 (1990) 345.
[24] A.L. Pruden, D.F. Ollis, J. Catal. 82 (1983) 404.
[25] W.A. Jacoby, M.R. Nimlos, D.M. Blake, Environ. Sci. Technol. 28 (1994) 1661.
[26] S. Suárez, J.M. Coronado, R. Portela, J.C. Martín, M. Yates, P. Avila, B. Sanchez, Environ. Sci. Technol. 42 (2008) 5892.
[27] J. Blanco, A. Romero, EP Patent 0978313A1, 2000.
[28] J.M. Coronado, S. Suárez, P. Portela, B. Sanchez, J. Adv. Oxid. Tech. 11 (2) (2008) 362.

[29] G.R. Hunt, Geophysics 42 (3) (1997) 501.
[30] R.N. Clark, Spectroscopy of rocks and minerals, and principles of spectroscopy, in: A.N. Rencz (Ed.), Manual of Remote Sensing, Remote Sensing for the Earth Sciences, vol. 3, John Wiley and Sons, New York, 1999 , pp. 3–58 (Chapter 1).
[31] R.N. Clark, T.V.V. King, M. Klejwa, G. Swayze, N. Vergo, J. Geophys. Res. 95 (B8) (1990) 12653.
[32] D.M. Sherman, Crystal chemistry, electronic structures and spectra of Fe sites in clay minerals, in: L.M. Coyne, S.W.S. McKeever, D.F. Drake (Eds.), Spectroscopic Characterization of Minerals and Their Surfaces, American Chemical Society, Washington DC, 1990, pp. 284–309.
[33] B. Sánchez, J.M. Coronado, R. Candal, R. Portela, I. Tejedor, M.A. Anderson, D. Tompkins, T. Lee, Appl. Catal. B 66 (2006) 295.
[34] W.A. Jacoby, D.M. Blake, R.D. Noble, C.A. Koval, J. Catal. 157 (1995) 87.